Simulation framework for activity recognition and benchmarking in different radar geometries

Zhou, Boyu ; Lin, Yier; Le Kernec, Julien; Yang, Shufan; Fioranelli, Francesco; Romain, Olivier; Zhao, Zhiqin

DOI
10.1049/rsn2.12049

Publication date
2021

Document Version
Final published version

Published in
IET Radar, Sonar and Navigation

Received: 15 March 2020 | Revised: 22 November 2020 | Accepted: 24 November 2020

DOI: 10.1049/rsn2.12049

IET Radar, Sonar & Navigation

The Institution of Engineering and Technology WILEY

ORIGINAL RESEARCH PAPER

Simulation framework for activity recognition and benchmarking in different radar geometries

Boyu Zhou[1] | **Yier Lin**[1] | **Julien Le Kernec**[1,2,3] | **Shufan Yang**[2] | **Francesco Fioranelli**[4] | **Olivier Romain**[3] | **Zhiqin Zhao**[1]

[1]School of Information and Communication, University of Electronic Science and Technology of China, Chengdu, China

[2]James Watt School of Engineering, University of Glasgow, Glasgow, UK

[3]Signal and Information Processing Lab, University-Cergy-Pontoise, Cergy-Pontoise, France

[4]Department of Microelectronics, MS3-Microwave Sensing Signals and Systems, Delft, The Netherlands

Correspondence

Julien Le Kernec, School of Information and Communication, University of Electronic Science and Technology of China, Chengdu, China.
Email: julien.lekernec@glasgow.ac.uk

Funding information

British Council, Grant/Award Number: 515095884, 514739586; Campus France, Grant/Award Number: 44764WK; PHCAlliance France-UK UK EPSRC, Grant/Award Number: INSHEPEP/R041679/1

Abstract

Radar micro-Doppler signatures have been proposed for human monitoring and activity classification for surveillance and outdoor security, as well as for ambient assisted living in healthcare-related applications. A known issue is the performance reduction when the target is moving tangentially to the line of sight of the radar. Multiple techniques have been proposed to address this, such as multistatic radar and to some extent, interferometric (IF) radar. A simulator is presented to generate synthetic data representative of eight radar systems (monostatic, circular multistatic and in-line multistatic [IM] and IF) to quantify classification performances as a function of aspect angles and deployment geometries. This simulator allows an unbiased performance evaluation of different radar systems. Six human activities are considered with signatures originating from motion-captured data of 14 different subjects. The classification performances are analysed as a function of aspect angles ranging from 0° to 90° per activity and overall. It demonstrates that IF configurations are more robust than IM configurations. However, IM performs better at angles below 55° before IF configurations take over.

1 | INTRODUCTION

Radar signatures, in particular, micro-Doppler (mD) signatures, have attracted significant interests for classification of human activities, both in the outdoor environments for security and surveillance, and in the indoor environments for healthcare and assisted living applications [1,2].

An issue for classification based on mD signatures is the performance reduction for targets' trajectories tangential to the radar line of sight, as the mD frequency shifts are reduced, and it is challenging to extract informative features from the data. For example, Tahmoush [3] showed that mD classification performance dropped to 40% at high aspect angles, and references [4–7] analysed the classification performance and limitations due to the aspect angle. When the target is not walking in the radial direction, depending on the aspect angle, the salient features for classification may change, and the accuracy of classification reduces as the target velocity gets closer to the tangential direction. In [8], a monostatic radar is used to classify human activities at 0°, 45° and 90° yielding 96%, 97% and 91% accuracy, respectively, using convolutional neural networks (CNN). This was increased to 98% when the directions are fused, but this would require four separate radar systems to acquire data sequentially to avoid interference as opposed to using multiple views simultaneously with multistatic radar.

As monostatic radar can only observe well the radial component of the mD signal, multiple cooperating radar sensors have been suggested to enhance the classification of mD signatures. This provides additional information from multistatic perspectives, at the price of increased system complexity to synchronise the different nodes [9–11] separated by a baseline (the distance between nodes, e.g. transmitter to receiver in the bistatic case). For example, in [12], the authors proposed two methods for personnel recognition and gait classification using deep CNN based on measured multistatic radar (in-line with a baseline of 50 m – 3 receivers and a transmitter at the centre) mD

signatures and obtained 99% accuracy and showed superior performances compared to any of the nodes separately by 5% to 8%. However, the target aspect angle exploration is limited to 15°. Multistatic radar with fusion is shown in [13] for aspect angles at 0°, 30°, 60°, 120°, 180°, 210°, 240° and 300° with respect to the central radar node. The radar configuration is in-line with a baseline of 40 m (3 receivers and 1 transmitter on the far right with the 3rd receiver). This showed that significant performance accuracy could be achieved when using separate classification at each node followed by a voting procedure to reach the final decision, which was beneficial, especially at aspect angles less favourable for mD feature detection. This method achieved about 90% accuracy using feature extraction cepstrum coefficients, principal component analysis, K-nearest neighbour and Naïve Bayes classifiers. An early implementation of simulated multistatic radar mD signatures from the Boulic model [14] for walk is presented in [15]. It shows how noisier data and the fusion of the mD signatures of several nodes together may improve the quality/clarity of the mD signature in comparison to only one node considering aspect angles at 0°, 30° and 75°.

Interferometric (IF) information has also been suggested as an alternative/complementary technique. Nanzer [16], presented an analysis of the angular velocity measurement of a person who is walking via a millimetre-wave correlation interferometer, which also covered the IF measurement theory of angular velocity and the frequency response simulations of a walking human participant. The IF channel provided information about the target angular velocity. This IF signature is more pronounced as the baseline between the antennas is increasing. In [17], a 29.5 GHz IF radar prototype was tested, and IF signatures of a person walking clockwise or counter-clockwise were generated experimentally validating the theory developed in [16]. In [18], the frequency shifts imparted on the signal in both Doppler and IF detection modes were measured in the time-frequency domain. They showed that as the trajectory moved from a completely radial motion to completely angular motion, the Doppler frequency shift decreased.

In contrast, the IF frequency shift increased for the walking action. Hence, these two detection modes can represent complementary measurements, improving the ability to measure the motion of randomly moving objects. Reference [19] showed that the IF radar signal is mathematically similar to that of a Doppler radar and that the time-frequency responses of both modes (mD and IF) to a walking human had similar characteristics for classification purposes. In [20], the use of this technique was also applied to unmanned aerial vehicles (UAVs), showing that when the mD signature diminished, the IF signature increased, therefore, maintaining salient information at any aspect angle. The authors in [21] presented a Viterbi algorithm to estimate the instantaneous frequency, and the echo signals decomposed with intrinsic chirp component decomposition. These resulting separated signatures were then analysed through feature extraction to recover the target trajectory in the IF plane. In [22], an analytical demonstration backed by simulations and experiments, the effectiveness of the IF measurement when the blades of a UAV were rotating in the plane 90° from the radial direction was demonstrated. All these studies show promise for classification purposes using the IF modality, and this is further reinforced for human gesture recognition with experimental data in [23]. The study is missing a benchmark to evaluate the effectiveness of the IF sensing modality against monostatic and multistatic radar for varying aspect angles.

The focus of this study is on the benchmarking of human activity recognition using different radar geometries with respect to aspect angle. Improving neural networks for human activity recognition or deriving detection estimation theories is out of the scope of this study.

Figure 1 summarises the state-of-the-art in human activity recognition using radar with either simulated or measured data, considering the different domains of radar data representations based on [1,2,6,24,25]. The research community has mainly focused on mD signatures for human radar classification. Still, this domain has shown limitations to distinguish between activities showing similar radial acceleration with respect to the radar, a.k.a., confusers. Multistatic radar has been used to enhance classification accuracy with confusers and to tackle aspect angle issues, but the IF sensing modalities have seldom been used in the study. The specific contributions of the proposed bespoke simulator are:

- The benchmarking of the classification accuracy of eight radar geometries per activity and overall as a function of aspect angle ranging from 0° to 90° for six different activities.
- The robustness analysis of the reduction of the baseline of in-line multistatic (IM) radar and IF radar with respect to aspect angle for indoor use.

This enables us to predict and compare classification performances for different radar approaches and aspect angles, providing useful pointers for practical deployment and most favourable geometries before performing experimental study.

The focus of this study is on the Doppler-time representations (mD signatures) and by association IF data often seen as complementary and alternative to mD. Several techniques have been used on mD signatures as it represents the majority of contributions on human activity recognition with radar to date. The classification techniques include Bi-LSTM [25], LSTM [26], SGRU [27], SAE, CAE [2], CNN [28,29] and MFCC/FWCC [6,29] leading to increasingly better performances. One aspect of deep learning that seems common to all the reviewed studies is the importance of having networks that converge and do not overfit to the training data. This is further reinforced by recent study on simulated data to improve the performances of deep neural networks for transfer learning to improve accuracy for a limited amount of data, as is usually the case in radar [30]. The authors tested the accuracy of the networks depending on the depth of the networks and have concluded that shallower networks performed better if data are not available or augmented to the required amount. For this study, a shallow CNN network (LeNet-5 [31]) has been selected to perform the transfer learning from optical recognition to radar activity recognition.

The remainder of this study is organised as follows. Section 2 describes the methodology to establish the simulation

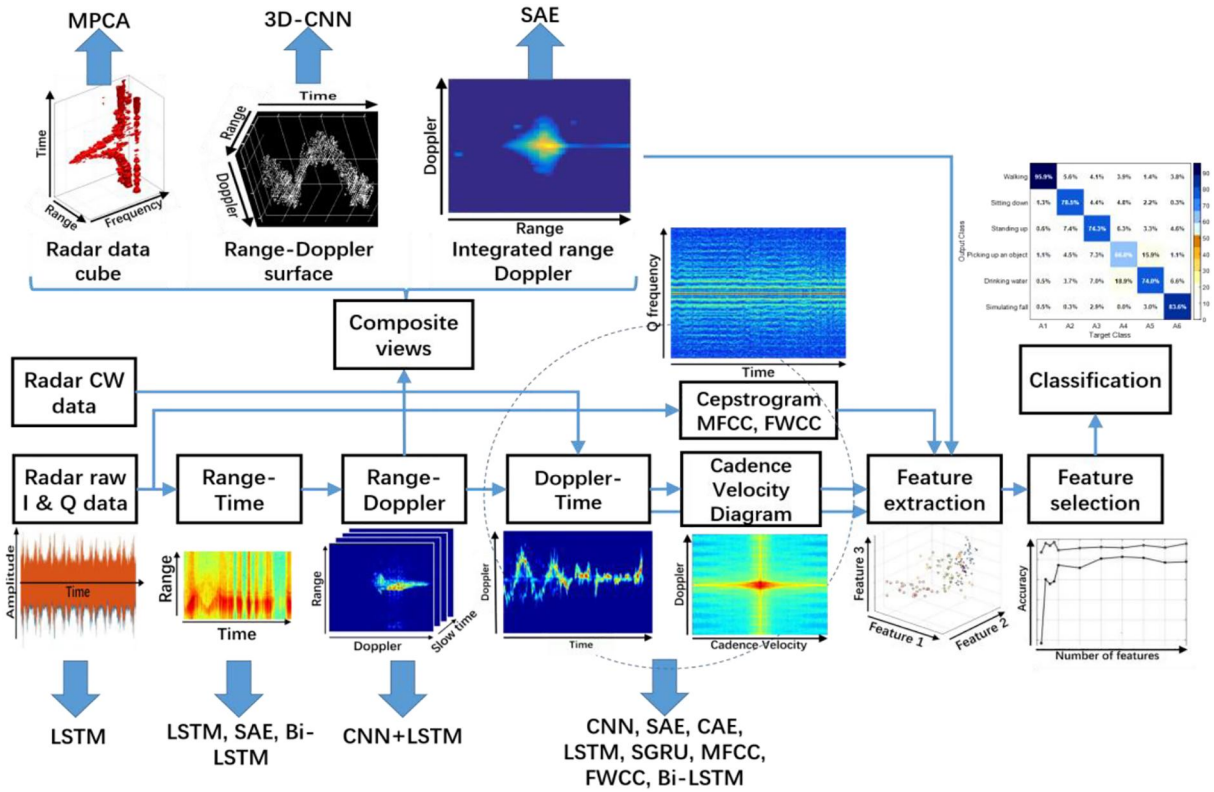

FIGURE 1 State-of-the-art overview of the human activity classification machine-learning algorithms with radar as a sensing modality [1,2,6,24,25] – LSTM, long short-term memory; Bi-LSTM, bi-directional LSTM; SAE, stacked autoencoders; CAE, convolutional autoencoders; SGRU, stacked gated recurrent units; MFCC, mel-frequency cepstrum coefficients; FWCC, frequency-warped cepstrum coefficients; CNN, convolutional neural network; 3D-CNN, 3-dimensional CNN; MPCA, multilinear principal component analysis

and classification framework. Section 3 presents the kinematic validation of the simulator. Section 4 presents different frequency responses and compares the results between the eight radar systems. Finally, conclusions are given in Section 5.

2 | METHODOLOGY OF THE SIMULATOR

A framework to simulate and compare performances of eight radar systems, was developed, including monostatic radar (mono): relying on mD signatures from a single mono radar node; circular multistatic radar (CM) (Figure 2(a)): using three separate nodes, whose results are fused for classification purposes using a majority voting approach; IM radar (Figure 2(b) *black* and *red*): using three separate nodes with baselines of 2 (IM2), 5 (IM5) and 10 m (IM10), whose results are fused for classification purposes using a majority voting approach; and IF radar (Figure 2(b) *black* and *blue*): using two receivers with baselines of 2 (IF2), 5 (IF5) and 10 m (IF10), whose results are fused with their IF response for classification using a majority voting approach.

Figure 3 shows the expected Doppler shifts for a carrier frequency of 9.8 GHz for a target at 1 m/s at the centre of the scene at varying aspect angles based on the theory described in [11,13]. The circular configuration was chosen at 0°, 45° and 90° as is offered more diversity in Doppler shifts for a more robust classification compared to narrower bistatic angles with a transmitter placement on the side as in [15]. The in-line configuration is inspired by [12] and Figure 3(a) shows the most extensive variation in Doppler shifts with a baseline of 10 m. As for the IF channel, the configuration is inspired by [19].

The performance comparison is based on the accuracy of classification for six human motions where the aspect angle θ between the target heading and the radar line of sight changes from 0° to 90° with 5° per step in rotation. The details of the geometry of the different radar setups are shown in Figure 2 and associated Doppler shift at the three receivers are shown in Figure 3. It is important to note that the target may be translating, and the aspect angle does not remain constant. Instead, the heading of the target is considered to define the aspect angle.

The six classes of motions considered include (I) walking; (II) forward jumping; (III) kicking; (IV) sitting and standing; (V) running; (VI) walking on uneven terrain. These data originate from the Carnegie Mellon (CMU) motion capture (MoCap) database [28,32], or the HDM05MoCap database [33]. Motion data in ASF/AMC format were used since this kind of skeleton-based data can comprise an explicit skeleton structure and also ensure that the bone lengths will be constant in the movement [28]. Motion data for head, torso, pelvis, legs, feet, arms and hands were used to simulate radar returns.

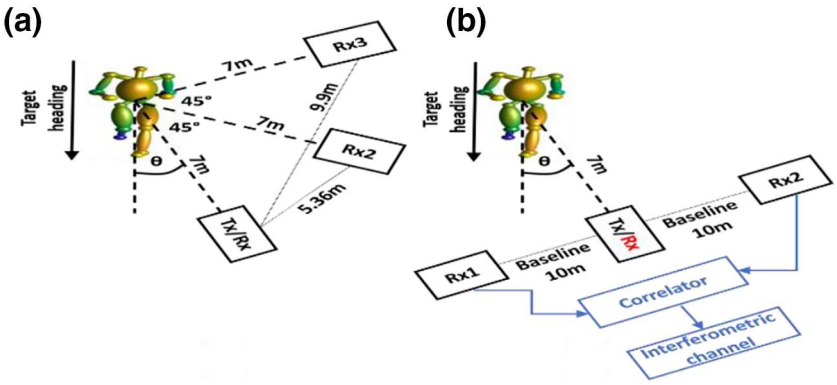

FIGURE 2 The simulation geometry for: (a) multistatic radar system—circular configuration and (b) interferometric radar system (*black* and *blue*) and multistatic radar—in-line configuration (*black* and *red*)

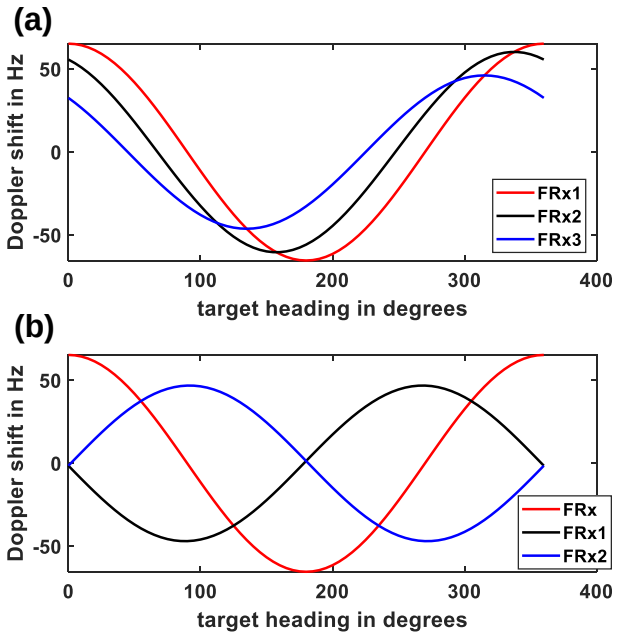

FIGURE 3 The expected Doppler shifts for: (a) the CM configuration with nodes at 0°, 45° and 90° and (b) the in-line configuration with a 10 m baseline (Rx_1/Rx_2 have the same Doppler shifts in the interferometric case) for a carrier frequency of 9.8 GHz

The motion data was originally captured at 120 frames per second in the database [28]. To simulate the Doppler frequency shift without aliasing, the sampling frequency was upsampled to 2 kHz before the simulation. The animation of human movement code was modified from the baseline MATLAB code provided by Chen [34], in particular, to generate multistatic and IF signals and signatures. Furthermore, the simulations are based on an accurate simulation of human motion based on motion-captured data which is captured from live volunteers [28–33]. Therefore, the kinematics of the human activities reflect natural movements. The radar signatures are based on proven simulation methods from the seminal work [34], which is extended using analytical equations for RCS in mono and bistatic configurations from [35,36]. At last, the theoretical frameworks for the bistatic and IF channels were demonstrated in [11,16–20]. The radar simulation parameters are carrier frequency 9.8 GHz, bandwidth 400 MHz and distance to target at the centre of the scene 7 m.

The resulting IF and Doppler responses are both processed in the time-frequency domain using hort-time Fourier transform (STFT). The STFT separates the time-varying signal into shorter segments using overlapped Gaussian windows with a length of 256 samples (128 ms at 2 kHz pulse repetition period).

A total of 88 different motion files performed by 14 subjects from the CMU database were simulated to generate the training and testing datasets. These motion files were used to generate the frequency responses at different aspect angles. It was not possible to have all six actions all the time from the same subject due to the intrinsic limitations of this dataset. Samples from every trial data were divided as 1-second long snapshots to increase the size of the dataset. Every class has 80 samples, and hence, the total samples are 480 (Table 1). Around 75% of the data was used for training, and 25% for testing.

CNNs use spectrograms/interferograms as input for classification and extract spatial features automatically. The mono radar system relies only on single mD signatures. The IF radar system implemented majority voting [37] as a decision-level fusion mechanism on the output labels from two mD signatures, and one IF frequency response. Therefore, it needs three separate CNNs. The CM/IM radar system also utilised the same fusion mechanism from three mD signatures from different radar nodes, hence it also needs three CNNs. In total, in every tested scenario, one CNN was trained per channel using the corresponding frequency responses.

The same network structure, as shown in Figure 4, was adopted in all of the CNNs with only small differences in the hyperparameters, as given in Table 2. This structure was inspired from LeNet-5 CNNs framework [31], and it comprises two convolutional layers, two Max pooling layers and two fully connected layers and can run from a classic laptop without the support of a graphics processing unit.

3 | SIMULATOR KINEMATIC FIDELITY

The kinematic validity of the simulator is demonstrated using mono measurements collected by utilising an off-the-shelf frequency-modulated continuous wave radar system in an indoor meeting room at the University of Glasgow, where

TABLE 1 Summary of motion data samples from CMU

Actions	Number of subjects	Number of files	Training set	Testing set
(I) Walking	3 (subject 02,07,08)	18	60	20
(II) Forward jumping	5 (subject 13,16,83,91,105)	23	60	20
(III) Kicking	1 (subject 144)	4	60	20
(IV) Sitting and standing	2 (subject 13,13)	9	60	20
(V) Running	2 (subject 09,35)	21	60	20
(VI) Walking on uneven terrain	1 (subject 36)	13	60	20

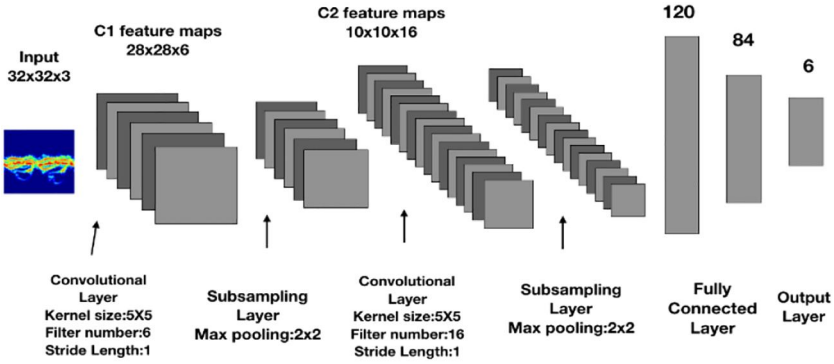

FIGURE 4 Structure of CNN used in this article as a classifier

TABLE 2 Hyperparameters for CNN

Hyperparameters	Value
Learning rate	0.012 ~ 0.013
Mini batch size	24
L2 Regularisation ratio	0.0005
Dropout rate	0.5
Solver	Stochastic gradient descent
Momentum	0.9
Mini batch size	16
Max epochs	150

multiple pieces of furniture such as chairs, tables, cupboards, blackboards and computers were present. The equipment and experimental scene are the same as those in [7,38]. The radar AncortekSDR-kit 580AD was operated at 5.8 GHz, with an instantaneous bandwidth of 400 MHz and a chirp duration of 1 ms (Doppler frequency range of ±500 Hz). The transmitted power of the radar was +19 dBm, and two linearly polarised Yagi antennas (17 dBi, beamwidth of 24° in azimuth and elevation). The antennas were located at a height of 1.2 m to aim at the torso of the human subjects, which provided the strongest contribution to the mD signature. The separation between the transmitter and receiver antennas was 40 cm. The experimental data collected from one volunteer performing four different activities (walking, sitting and standing, circling arms, bending) at 0° are analysed. The four activities are the same in the simulation. The distance between the radar and the target is consistent between experiments and simulations. CM/IM or IF geometries could not be measured due to a lack of suitable experimental equipment.

The mD signatures are segmented in 0.5s windows, and five hand-made features are selected to compare the simulated samples with the experimental samples centroid, entropy, skewness, mean and standard deviation of energy curves looking at their means and variances [35]. Thousand and two hundred samples were obtained per activity from the measured data, totalling 4800 samples. We generated the same number of samples in simulation for validation using a subject with a similar build. A quantitative comparison of simulated and measured spectrograms at 0° is shown in Table 3. The statistics of the five aforementioned features extracted from the simulated/measured spectrograms are based on a simulator validation presented in [39]. The mean and variance of features extracted from every activity are calculated for all the samples were seen to be comparable.

Based on this qualitative assessment of mono signatures, methodology and literature, the bespoke simulator is assumed to be providing signatures that are reflective of the physical phenomena with kinematic fidelity. This bespoke simulator does not use generative adversarial networks to generate signatures, as can be seen in [2]. The kinematic fidelity of the signatures cannot be altered, which could misrepresent the radar phenomenology, such as abnormal periodicity for a regular walker without a gait impediment, abnormal limb velocity lower than torso velocity or Doppler frequencies not matching the direction of movement.

TABLE 3 Statistical properties of extracted features from simulated and measured spectrograms at 0°

Features	Simulated mean	Simulated variance	Measured data	Measured variance
Walking				
Centroid	0.0077	1.6933×10^{-4}	0.0073	2.1802×10^{-4}
Entropy	1.9988	0.0206	2.6491	0.2850
Skewness	11.8347	0.0467	11.3217	0.1390
Mean of energy curves	-2.7207×10^{-15}	1.1706×10^{-13}	6.0125×10^{-16}	6.2340×10^{-14}
Standard deviation of energy curves	55.0759	2.1238	63.9661	4.6087
Sitting and standing				
Centroid	0.0038	0.0038	0.0038	0.0038
Entropy	1.1529	1.1534	1.1154	1.1163
Skewness	5.7820	5.7843	5.7806	5.7820
Mean of energy curves	2.7491×10^{-16}	7.9909×10^{-14}	3.5279×10^{-16}	6.5693×10^{-14}
Standard deviation of energy curves	26.0198	26.0586	39.5610	39.7027
Circling arms				
Centroid	0.0026	0.0036	0.0026	0.0036
Entropy	0.6941	0.9822	0.7031	0.9950
Skewness	3.9129	5.5346	3.9125	5.5341
Mean of energy curves	3.0268×10^{-16}	6.1216×10^{-14}	1.5926×10^{-15}	6.6474×10^{-14}
Standard deviation of energy curves	17.6108	24.9513	22.9059	32.4629
Bending				
Centroid	0.0018	0.0031	0.0019	0.0033
Entropy	0.6058	1.0520	0.5585	0.9677
Skewness	2.8474	4.9326	2.9025	5.0278
Mean of energy curves	-3.6220×10^{-16}	3.9546×10^{-14}	-6.1519×10^{-16}	5.1257×10^{-14}
Standard deviation of energy curves	12.5474	21.7683	16.6133	28.8338

4 | RESULTS AND DISCUSSIONS

4.1 | Micro-Doppler and interferometric responses examples

For all eight radar systems, the signatures for each of the receivers were captured from 0° to 90° with 5° steps in rotation. This section presents some examples of the signatures to visualise the phenomenology better. Figure 5 shows the mD signatures of the mono radar system at three aspect angles 0°, 45° and 90°. It can be observed from the mD signatures that the Doppler spread and mean decrease as the aspect angle in rotation increases from 0° to 90°. At 90°, the action is barely distinguishable.

In Figure 5, the mD signatures obtained with the CM radar system at receiver 3 (Rx_3) as the aspect angle evolves from 0° to 90°. Different bistatic angles in CM/IM configurations offer different results. It can be observed that the IF channel increases in amplitude as the aspect angle increases from 0° to 90°. Also, the greater the baseline, the larger the amplitude registered as the aspect angle increases.

4.2 | Comparison of different radar systems

These eight radar geometries were compared in classification accuracy of individual activities I to VI in Figures 6 and 7 and the overall accuracy in Figure 8 for the scenarios where the aspect angle changes from 0° to 90° with 5° steps. In every chosen aspect angle, every network associated with each radar channel was repeatedly trained 10 times through cross-validation, and then the decision level information was fused through majority voting.

Table 4 shows an analysis of the best configuration per activity/overall per aspect angle.

4.2.1 | Mono vs. IF10

Mono shows comparable performance in all kinds of motion with IF10 up to 30° with an overall accuracy difference under 2% up to 30°. It only outperforms IF10 by 1% for walking (I) at 5° and for sitting (IV) at 25°. At 35°, there is an obvious

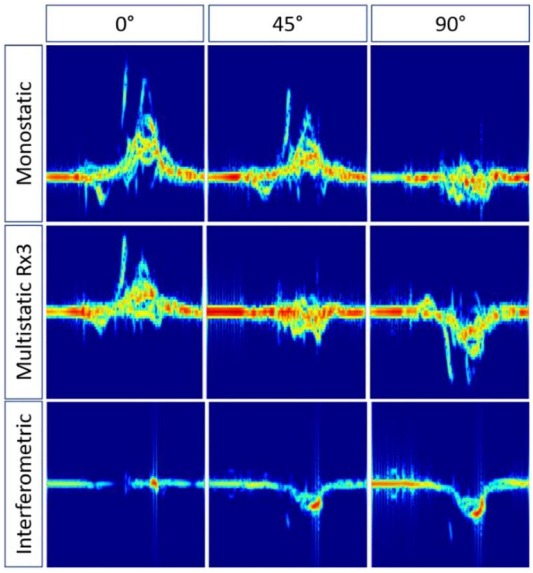

FIGURE 5 Simulated radar returns for action (II): (a) mD signatures from the mono radar at aspect angles 0°, 45° and 90°; (b) simulated mD signatures from the multistatic radar at receiver 3 (bistatic angle 90°) at aspect angle 0°, 45° and 90° and (c) frequency responses from the interferometric radar channel with a 10-m baseline at 0°, 45°and 90°

decrease in accuracy in every kind of motion, especially in walking on uneven terrain (VI) (∼0.11). The mean accuracy increase of walking on uneven terrain varies between 7% and 31% (at 85°). Although mono performs best for walking (I) and performs better in walking (I) and sitting and standing (IV) compared to other activities at 90° with ∼84%, IF10 has a ∼13% accuracy increase at the same angle. The overall accuracy increase of IF10 from 30° is at least 2.5% and up to 18.5% at 85°.

4.2.2 | CM vs. IF10

CM configuration shows comparable performance in all kinds of motion with IF10 before 40° with ±1% accuracy difference. In most of aspect angle schemes, kicking (III) has the best mean accuracy in CM configuration. The accuracy of IF10 in kicking (III) increases from 40° by at least 1% at 45° and 65° to 8% at 90°. By contrast, walking on uneven terrain (VI) has the worst mean accuracy in CM and IF10 configurations in almost all aspect angles. The accuracy of IF10 increases by at least 3% at 40° and up to 14% at 60°. The IF10 has the biggest accuracy increase in walking on uneven terrain (VI). From 40°, its value increases by at least 3% at 70° up to 19% at 85° with some fluctuations.

4.2.3 | IM10 vs. IF10

IM10 shows better performance compared with IF10 in most cases before 55° with an overall variation under ±1%. IM10 has the worst performance in walking on uneven terrain (VI) where the mean accuracy decreases to 88% at 90° where IF10 shows an increase of 7%. IF10 from 55° consistently equates or outperforms IM10 by up to 2% for walking (I), up to 5% for forward jumping (II), up to 3% for sitting and standing (IV) and 8% for walking on uneven terrain (VI). From 55° to 70°, the overall increase in accuracy provided by IF10 is up to 2%. From 75° to 90°, the contrast is increasing in accuracy with improvements up to 10% per activity and 4.3% overall compared with IM10. In terms of robustness of classification, IM10 has no standard deviation for walking (I) until 50° (55° for IF10), forward jumping (II) and running (V) until 40° (10° and 15° respectively for IF10) and kicking (III) until 70°. Both of them have very low standard deviations in cross-validation, but IF10 [0.37; 1.17] has improved stability over IM10 [0.91; 1.83] from 70° to 90°.

IF10 clearly outperforms the mono configuration at all angles. Whereas the CM configuration shows comparable performances up to 40°, the IF10 dominates in performance. The IM10 configuration dominates slightly at angles up to 50° and then the IF10 configuration is dominant slightly at angles between 55° and 70° and then outperforms clearly at high angles 75° to 90°. These results have been obtained with a large baseline 10 m. We, therefore, need to test the robustness of the IM/IF configurations with smaller baselines. This is supported by the analysis shown in Table 4.

4.2.4 | IF5 vs. IF10

IF5 has very similar classification accuracy with IF10, especially in walking (I), kicking (III) and running (V) with up to ±2% difference. IF5 shows some minor improvements in accuracy overall at 20°, 25°, 45°, 70° and 90° up to 0.34%. IF5 shows a degradation in performance with angles increasing and its performance in walking on uneven terrain (VI) shows the most apparent decrease with mean accuracy decreasing to 94% at 90°. By contrast, IF10 shows a stable performance in walking on uneven terrain (VI) with a little fluctuation around 96%. IF5 has a graceful reduction in performance lower by up to 1% overall compared with IF10. The degradation is most severe [0.8; 1]% at 40, 55-65 and 75°.

4.2.5 | IF2 vs. IF10

IF2 configuration shows comparable classification accuracy up to 55° with a degradation of up to 2% compared with IF10. From 60°, the performance of IF2 decreases drastically especially in walking on uneven terrain (VI) with a degradation ranging from 9.6% to 18% and, sitting and standing (IV) with a degradation ranging from 7% to 12%. The accuracy gap in forward jumping (II) increases to 10% at 85° and 90°. The overall classification accuracy of IF2 degrades rapidly from 60° from 4.7 up to 8.5% compared to IF10.

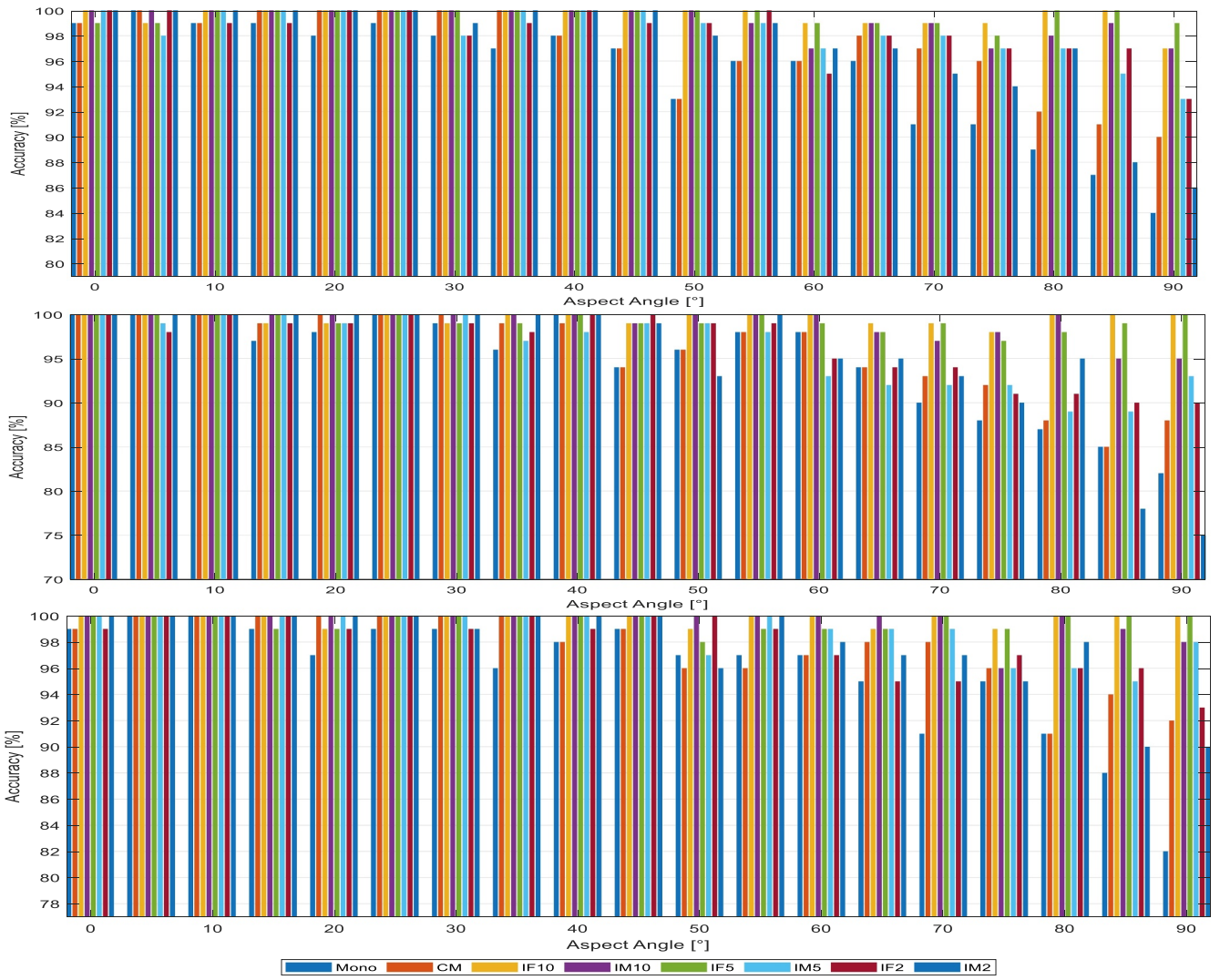

FIGURE 6 Comparison of the accuracy of the eight geometries (mono, CM, IF10, IM10, IF5, IM5, IF2, IM2) for: (a) activity I—the IF configuration dominates in high aspect angles (>55°) and IM and IF have 100% recognition up to 50°, (b) activity II—the IF configuration dominates or equates IM in high aspect angles (>45°), and IM dominates or equates IF up to 40° and (c) activity III—the IF configuration dominates or equates IM in high aspect angles (>65°), and IM dominates or equates IF up to 65° for the scenarios where the aspect angle changes from 0° to 90° with 5° steps

4.2.6 | IM5 vs. IM10

IM5 configuration shows similar classification accuracy with a degradation of up to 1.8% compared with IM10 from 0° to 55°. The overall accuracy from 60° to 90° experiences a degradation ranging from 3.5% to 6.4%. The performance of IM5 in walking on uneven terrain (VI) is not better than IM10 in all aspect angles. The degradation is most notable for walking on uneven terrain (VI) with 12.4% for IM5 compared to IM10 at 80° and forward jumping (II) with 11% degradation at 80°.

4.2.7 | IM2 vs. IM10

IM2 shows similar performance with IM10 before 25° with ±0.3% difference. This degradation in performance for IM2 is up to 5% from 30° to 55° compared to IM10. From 60°, the overall accuracy for IM2 drops from 5% to 15% compared to IM10. After 25°, the IM2 configuration is identical or worse than IM10 in all motions, and the accuracy gap between them increases as the aspect angle increases. The accuracy gap in jumping forward (II) is noticeable where the increase ranges from 7% at 50° to 21% at 90°. IM10 also shows a visible increase in walking on uneven terrain (VI) where the accuracy gap increases to 19% at 90° from 1% at 25°.

4.2.8 | IM5 vs. IF5

IM5 and IF5 show similar overall performance before 55° with ±1.3% difference. The degradation in overall accuracy for IM5 ranges from 3.4% to 8.3% compared to IF5 from 60°. IF5 shows better or equal performances compared to IM5 consistently in walking (I) from 5°, jumping forward (II) from

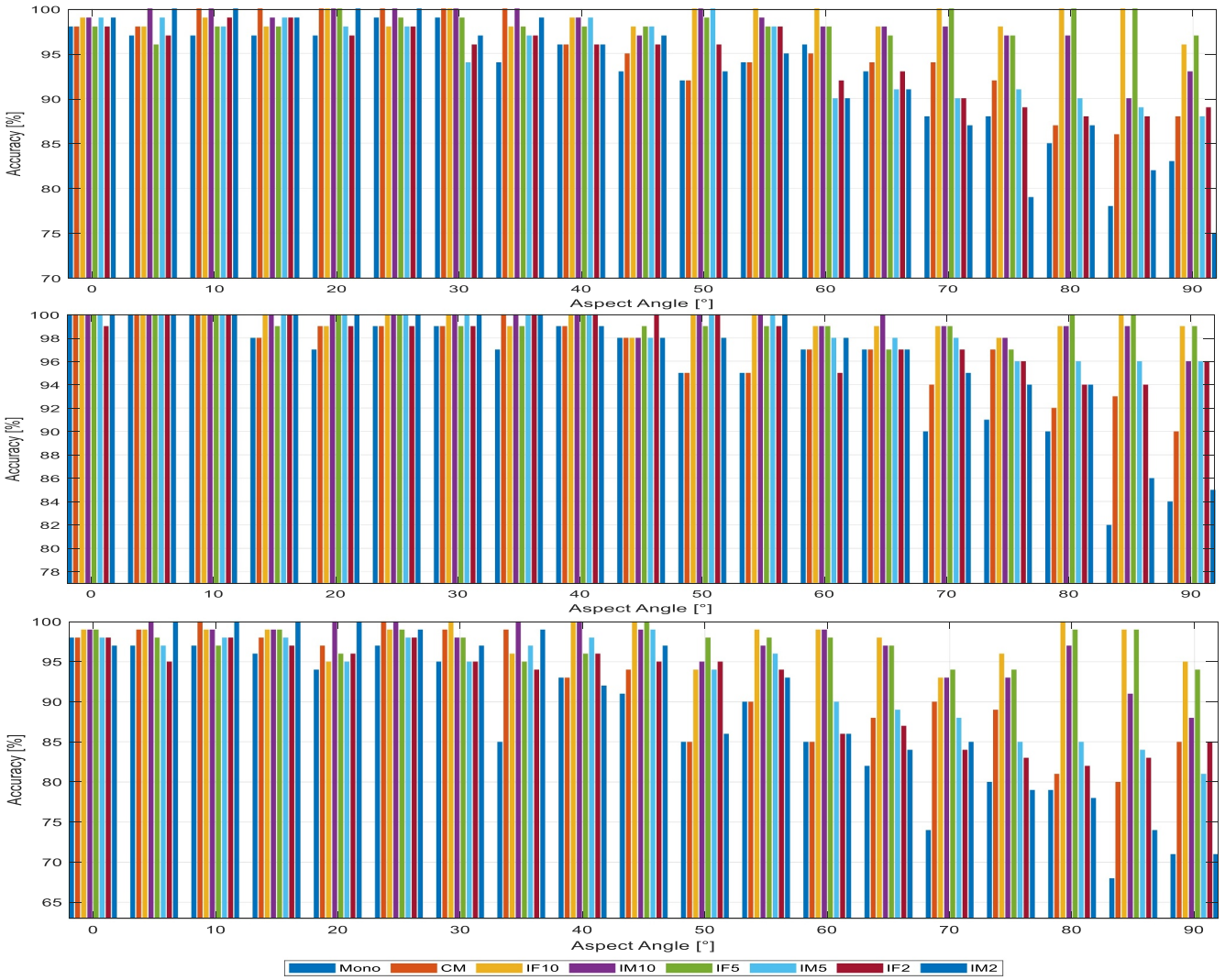

FIGURE 7 Comparison of the accuracy of the eight geometries (mono, CM, IF10, IM10, IF5, IM5, IF2, IM2) for: (a) activity IV—the IF configuration dominates or equates IM in high aspect angles (>50°) and at 45°, and IM dominates or equates IF up to 40° and at 50°, (b) activity V—the IF configuration dominates or equates IM in high aspect angles (>40°) except at 55° and 65° where IM dominates, and IM dominates or equates IF up to 40° and (c) activity VI—the IF configuration dominates or equates IM in high aspect angles (>40°), and IM dominates or equates IF up to 40° for the scenarios where the aspect angle changes from 0° to 90° with 5° steps

35°, kicking (III) from 60°, sitting and standing (IV) from 55°, running (V) from 70° and walking on uneven terrain (VI) from 45°. IF5 shows noticeable accuracy increases in walking on uneven terrain (VI) where the accuracy gap increases to 13.8% at 90° from 1% at 45°.

4.2.9 | IM2 vs. IF2

IM2 shows better performance than IF2 before 35° with an increase ranging from 0.33% to 1.7%. However, IF2 shows better performance or marginal degradation compared to IM2 from 40° to 80° from 0.7% degradation up to 4.2% improvement. IF2 shows the biggest accuracy increase at 85° and 90° in all six motions with at least 7.5% (I), 13.3% (II), 3.2% (III), 6.8% (IV), 8.5% (V) and 10.4% (VI) improvement, respectively. IF2 outperforms overall IM2 by 9.1% at 85° and 11% at 90°.

This confirms the IM configuration dominates at lower angles even if by a small margin and that IF dominates more significantly on higher angles overall because of the contributions of actions walking (I) and walking on uneven terrain (VI) as shown in Table 4.

5 | CONCLUSION

Eight radar systems (mono, CM, IF10, IM10, IF5, IM5, IF2, IM2), for six classes of motions (walking (I), forward jumping (II), kicking (III), sitting and standing (IV) and walking on uneven terrain (VI)) were simulated and compared in scenarios

TABLE 4 Analysis of the best configuration per activity/overall per aspect angle. The *greyed* out accuracy shows a dominant performance of IM configurations, whereas the *yellow* highlights show dominant performances for IF configurations per activity and for overall performances

	0	**5**	**10**	**15**	**20**	**25**	**30**	**35**	**40**	**45**	**50**	**55**	**60**	**65**	**70**	**75**	**80**	**85**	**90**
Config (I)	3,4,6,7,8	1,2,4,7,8	3,4,5,6,8	2,3,4,5,6,8	2,3,4,5,6,7,8	2,3,4,5,6,7,8	2,3,4,5	2,3,4,5,6,8	3,4,5,6,7,8	3,4,5,6,8	3,4,5	3,5,7	3,5	3,4,5	3,4,5	3	3,5	3,5	5
Acc (I)	100	100	100	100	100	100	100	100	100	100	100	100	99	99	99	99	100	100	99
Config (II)	All	1,2,3,4,5,8	All	4,5,6,8	2,4,8	All	2,4,6,8	3,4,8	1,3,4,5,7,8	7	3,4	3,4,5,8	3,4	3	3,5	3,4	3,4	3	3,5
Acc (II)	100	100	100	100	100	100	100	100	100	100	100	100	100	99	99	98	100	100	100
Config (III)	3,4,5,6,8	All	All	2,3,4,6,7,8	2,4,6,8	2,3,4,5,6,7,8	2,3,4,5,6	2,3,4,5,6,7,8	3,4,5,6,8	3,4,5,6,7,8	4,7	3,4,6,8	3,4	4	3,4,5	3,5	3,4,5	3,5	3,5
Acc (III)	100	100	100	100	100	100	100	100	100	100	100	100	100	100	100	99	100	100	100
Config (IV)	3,4,6,8	4,8	2,4,8	2	2,3,4,5,8	2,4,8	2,3,4	2,4	3,4,6	3,5,6	3,4,6	3	3	3,4	3,5	3	3,5	3,5	5
Acc (IV)	99	100	100	100	100	100	100	100	99	98	100	100	100	98	100	98	100	100	97
Config (V)	1,2,3,4,5,6,8	All	All	3,4,6,7,8	4,5,6,8	3,4,5,6,8	3,4,6,8	2,4,6,7,8	3,4,5,6,7	7	3,4,6,7	3,4,6,8	3,4,5	4	3,4,5	3,4	5	3,5	3,5
Acc (V)	100	100	100	100	100	100	100	100	100	100	100	100	99	100	99	98	100	100	99
Config (VI)	3,4,5	4,8	2,8	8	4,8	2,4	3	4	3,4	3,5	5	3	3,4	3	5	3	3	3	3
Acc (VI)	99	100	100	100	100	100	100	100	100	100	98	99	99	98	94	96	100	99	95
Config (avg)	3,4	4,8	8	8	4,8	4	3	4	3,4	5	4	3	3	3,4	5	3	3	3	5
Acc (avg)	99.7	100	100	99.8	100	100	99.8	100	99.8	99.3	99.2	99.8	99.5	98.7	98.5	98	99.8	99.8	98.2

Note: 1, Mono; 2, CM; 3, IF10; 4, IM10; 5, IF5; 6, IM5; 7, IF2; 8, IM2.

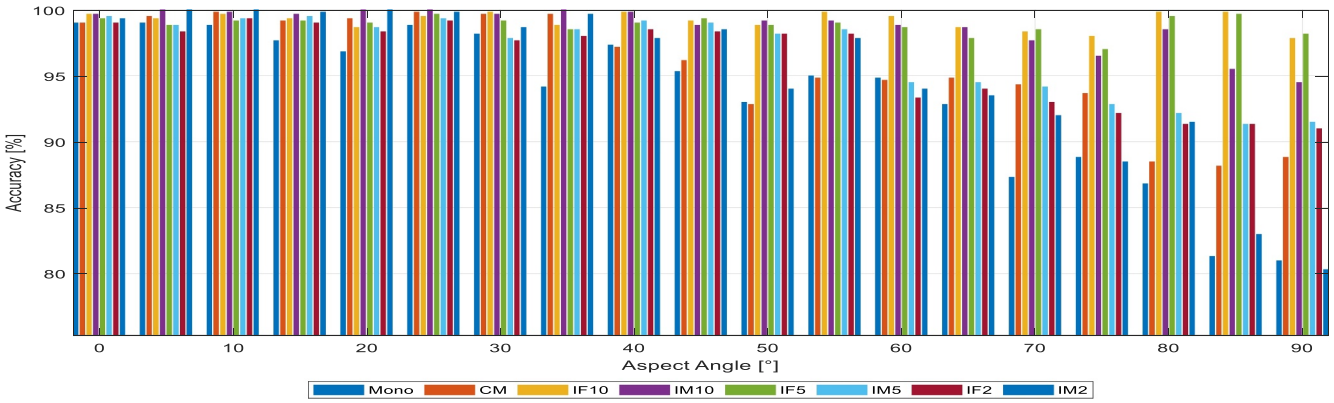

FIGURE 8 Comparison of the accuracy of the eight geometries (mono, CM, IF10, IM10, IF5, IM5, IF2, IM2) for all the activities for the scenarios where the aspect angle changes from 0° to 90° with 5°steps. The IM configuration outperforms slightly or equates the IF configuration for angles up to 55° for overall accuracy. The tendency changes to IF outperforming slightly or equating IM up to 70° and then at high aspect angles IF clearly outperforms the IM configuration. IF10 maintains an accuracy of over 97.58% (94.5% for IM10) overall and 97.08% with IF5 (91.3% for IM5). Even with a reduction in the baseline, the IF radar maintains good performance at high aspect angles

where the aspect angle to the heading of the target varies from 0° to 90° to the radar line of sight. A total of 88 different motion data files performed by 14 human subjects from CMU were simulated to generate corresponding spectrograms and interferograms. The simulator kinematic validity was demonstrated as well to ensure the fidelity of the simulations with respect to measured data. In every scenario, one CNN was trained per channel to achieve the tasks of classification and comparison. From the simulation results given in Section 4, the IF radar with 5 m or 10 m baseline is more robust in performance compared to IM with similar baselines. The IM configuration outperforms slightly or equates the IF configuration for angles up to 55° for overall accuracy. The tendency changes to IF outperforming slightly or equating IM up to 70° and then at high aspect angles, IF clearly outperforms the IM configuration.

IF10 maintains an accuracy of over 97.58% (94.5% for IM10) overall and 97.08% with IF5 (91.3% for IM5). Even with a reduction in the baseline, the IF radar maintains good performances at high aspect angles.

In contrast, the performance degradation for the IM configuration would not be acceptable for operational deployment considering indoor applications and would increase the cost of the system by adding another radar to cover the decrease in performance at high aspect angle or a different sensing modality. Additionally, for the IF configuration, the higher the carrier frequency, the smaller the baseline has to be to enjoy the same performances. With the advent of millimetre-wave technologies, a similar level of performances will be available with a much smaller form factor for indoor scenarios, whereas IM would require a significant baseline to maintain good performances and may not be suitable for indoor environments.

Future study will look at the feature level fusion for the implementation of classification to reduce the computational load, and lightweight implementation of the networks to reduce their size and time for training and inference.

There is scope for expansion and improvement of the bespoke simulator to increase realism through the incorporation of additional details and different movements. For example, an essential element to consider when simulating would be the antenna beam pattern and free space losses, as they do influence the results, especially for large baselines. The baselines considered here are rather large for indoor monitoring. Higher operational frequencies in the millimetre-wave region will result in much smaller baselines for more practical implementations in real life.

Furthermore, this study considered only one target in the field of view. If two or more targets are in the radar field of view, the correlation will entangle the signatures. Means to separate the targets from both channels and match them will need to be devised before the correlation operation to exploit the IF channel in multioccupancy scenarios fully.

ACKNOWLEDGMENTS

The authors would like to thank the British Council (grant515095884, 514739586), Campus France 44764WK—PHCAlliance France-UK, and the UK EPSRC (grant INSHEPEP/R041679/1) for their financial support.

ORCID

Julien Le Kernec https://orcid.org/0000-0003-2124-6803

REFERENCES

1. Kernec, J.L., et al.: Radar signal processing for sensing in assisted living: the challenges associated with real-time implementation of emerging algorithms. IEEE Signal Process. Mag. 36(4), 29–41 (2019). https://doi.org/10.1109/MSP.2019.2903715
2. Gurbuz, S.Z., Amin, M.G.: Radar-based human-motion recognition with deep learning: promising applications for indoor monitoring. IEEE Signal Process. Mag. 36(4), 16–28 (2019). https://doi.org/10.1109/MSP.2018.2890128
3. Tahmoush, D., Silvious, J.: Radar micro-Doppler for long range front-view gait recognition. In: EEE 3rd International Conference on Biometrics: Theory, Applications, and Systems. 28(30), 1–6, IEEE, Washington, DC (2009). https://doi.org/10.1109/BTAS.2009.5339049
4. Tekeli, B., Gurbuz, S.Z., Yuksel, M.: Information-theoretic feature selection for human micro-Doppler signature classification. IEEE Trans.

Geosci. Remote Sens. 54(5), 2749–2762 (2016). https://doi.org/10.1109/TGRS.2015.2505409
5. Çağlıyan, B., Gürbüz, S.Z.: Micro-Doppler-based human activity classification using the Mote-scale BumbleBee radar. IEEE Geosci. Remote Sens. Lett. 12(10), 2135–2139 (2015). https://doi.org/10.1109/LGRS.2015.2452946
6. Gürbüz, S.Z., et al.: Operational assessment and adaptive selection of micro-Doppler features. IET Radar Sonar Nav. 9(9), 1196–1204 (2015). https://doi.org/10.1049/iet-rsn.2015.0144
7. Kim, Y., Ling, H.: Human activity classification based on micro-Doppler signatures using a support vector machine. IEEE Trans. Geosci. Remote Sens. 47(5), 1328–1337 (2009). https://doi.org/10.1109/TGRS.2009.2012849
8. Parashar, K.N., et al.: Micro-Doppler feature extraction using convolutional auto-encoders for low latency target classification. In: IEEE RADAR conference (RadarConf), pp. 1739–1744 (2017). https://doi.org/10.1109/RADAR.2017.7944488
9. Fairchild, D.P., Narayanan, R.M.: Multistatic micro-Doppler radar for determining target orientation and activity classification. IEEE Trans. Aerosp. Electron. Syst. 52(1), 512–521 (2016). https://doi.org/10.1109/TAES.2015.130595
10. Fioranelli, F., Ritchie, M., Griffiths, H.: Centroid features for classification of armed/unarmed multiple personnel using multistatic human micro-Doppler. IET Radar Sonar Nav. 10(9), 1702–1710 (2016)
11. Willis, N.J.: Bistatic Radar, 2nd edition. Scitech publishing Inc. (2004)
12. Chen, Z., et al.: Personnel recognition and gait classification based on multistatic micro-Doppler signatures using deep convolutional neural networks. IEEE Geosci. Remote Sens. Lett. 15(5), 669–673 (2018). https://doi.org/10.1109/LGRS.2018.2806940
13. Fioranelli, F., Ritchie, M., Griffiths, H.: Aspect angle dependence and multistatic data fusion for micro-Doppler classification of armed/unarmed personnel. IET Radar Sonar Nav. 9(9), 1231–1239 (2015). https://doi.org/10.1049/iet-rsn.2015.0058
14. Boulic, R., Thalmann, N.M., Thalmann, D.: A global human walking model with real-time kinematic personification. Visual Comput. 6(6), 344–358 (1990/11/01 1990). https://doi.org/10.1007/bf01901021
15. Karabacak, C., Gürbüz, S.Z., Gürbüz, A.C.: Radar simulation of human micro-Doppler signature from video motion capture data. In: 21st Signal Processing and Communications Applications Conference (SIU), pp. 1–4 (2013). https://doi.org/10.1109/SIU.2013.6531365
16. Nanzer, J.A.: Interferometric measurement of the angular velocity of moving humans (SPIED efense, Security, and Sensing). SPIE (2012)
17. Nanzer, J.A., Kammerman, K., Zilevu, K.S.: A 29.5 GHz radar interferometer for measuring the angular velocity of moving objects. In: 2013 IEEE MTT-S International Microwave Symposium Digest (MTT), pp. 1–3 (2013). https://doi.org/10.1109/MWSYM.2013.6697333
18. Nanzer, J.A., Zilevu, K.S.: Dual interferometric-Doppler measurements of the radial and angular velocity of humans. IEEE Trans. Antennas Propag. 62(3), 1513–1517 (2014). https://doi.org/10.1109/TAP.2013.2296325
19. Nanzer, J.A.: Micro-motion signatures in radar angular velocity measurements. In: 2016 IEEE Radar Conference (RadarConf), pp. 1–4 (2016). https://doi.org/10.1109/RADAR.2016.7485234
20. Nanzer, J.A., Chen, V.C.: Microwave interferometric and Doppler radar measurements of a UAV. In: 2017 IEEE Radar Conference (RadarConf), pp. 1628–1633 (2017). https://doi.org/10.1109/RADAR.2017.7944468
21. Kang, W., Zhang, Y., Dong, X.: Micro-Doppler feature extraction for interferometric radar based on Viterbi algorithm and intrinsic chirp component decomposition. In: 2018 22nd International Microwave and Radar Conference (MIKON), pp. 508–511 (2018). https://doi.org/10.23919/MIKON.2018.8405271
22. Wang, X., et al.: Interferometric angular velocity measurement of rotating blades: Theoretical analysis, modeling and simulation study. IET Radar Sonar Nav. 13(3), 438–444 (2019). https://doi.org/10.1049/iet-rsn.2018.5205
23. Klinefelter, E., Nanzer, J.A.: Interferometric radar for spatially persistent gesture recognition in human-computer interaction. In: 2019 IEEE Radar Conference (RadarConf), pp. 1–5 (2019). https://doi.org/10.1109/RADAR.2019.8835739
24. Du, H., et al.: A three-dimensional deep learning framework for human behavior analysis using range-Doppler time points. IEEE Geosci. Remote Sens. Lett. 17(4), 1–5 (2019). https://doi.org/10.1109/LGRS.2019.2930636
25. Li, H., et al.: Bi-LSTM network for multimodal continuous human activity recognition and fall detection. IEEE Sens. J. 20(3), (2019). https://doi.org/10.1109/JSEN.2019.2946095
26. Yang, S., et al.: Human activities classification in a complex space using raw radar data. In: International Radar Conference, Toulon, France, pp. 23–27 (2019)
27. Wang, M., et al.: Human body and limb motion recognition via stacked gated recurrent units network. IET Radar Sonar Nav. 12(9), 1046–1051 (2018). https://doi.org/10.1049/iet-rsn.2018.5054
28. Lin, Y., et al.: Human activity classification with radar: Optimisation and noise robustness with iterative convolutional neural networks followed with random forests. IEEE Sens. J. 18(23), 9669–9681 (2018). https://doi.org/10.1109/JSEN.2018.2872849
29. Seyfioglu, M.S., et al.: DNN transfer learning from diversified micro-Doppler for motion classification. IEEE Trans. Aerosp. Electron. Syst. 55(5), 2164–2180 (2019). https://doi.org/10.1109/TAES.2018.2883847
30. Shrestha, A., et al.: Cross-frequency classification of indoor activities with DNN transfer learning. In: IEEE Radar Conference, Boston, MA, USA, pp. 22–26 (2019)
31. Lecun, Y., et al.: Gradient-based learning applied to document recognition. Proc. IEEE. 86(11), 2278–2324 (1998). https://doi.org/10.1109/5.726791
32. Lin, Y., Kernec, J.L.: Performance analysis of classification algorithms for activity recognition using micro-Doppler feature. In: 13th International Conference on Computational Intelligence And Security, CIS, Hong Kong, China, pp. 15–18 (2017)
33. Muller, M., et al.: Documentation Mocap Database HDM05. Institut fur informatik II Universitat Bonn D-53117, Bonn, Germany, CG (2007)
34. Chen, V.: The Micro-Doppler Effect in Radar. Artech House, London, Boston (2011)
35. Li, H., et al.: A multisensory approach for remote health monitoring of older people. IEEE J. Electromagn. RF Microw. Med. Biol. 2(2), 102–108 (2018). https://doi.org/10.1109/JERM.2018.2827099
36. Karabacak, C., et al.: Multi-aspect Angle Classification of Human Radar Signatures (SPIED efense, Security, and Sensing). SPIE (2013)
37. Erol, B., et al.: Simulation of human micro-Doppler signatures with Kinect sensor. In: 2014 IEEE Radar Conference vol. 19, pp. 0863–0868. IEEE, Cincinnati (2014). https://doi.org/10.1109/RADAR.2014.6875712
38. Crispin, J.W., Maffett, A.L.: Radar cross-section estimation for simple shapes. Proc. IEEE. 53(8), 833–848 (1965). https://doi.org/10.1109/PROC.1965.4062
39. Trott, K.D.: Stationary phase derivation for RCS of an ellipsoid. IEEE Antennas Wirel. Propag. Lett. 6, 240–243 (2007). https://doi.org/10.1109/LAWP.2007.891521

How to cite this article: Zhou B, Lin Y, Le Kernec J, et al. Simulation framework for activity recognition and benchmarking in different radar geometries. *IET Radar Sonar Navig.* 2021;15:390–401. https://doi.org/10.1049/rsn2.12049